# Enhanced multiferroic properties of Y and Mn codoped multiferroic BiFeO$_3$ nanoparticles

A. Mukherjee · S. Basu · L. A. W. Green ·
N. T. K. Thanh · M. Pal

**Abstract** Enhancement of multiferroic properties of bismuth ferrite (BFO) is a real challenge to the scientific community. We are able to achieve improved magnetic and electric properties in chemically prepared nanocrystalline BFO by virtue of the beneficial effect of Y and Mn codoping. Phase purity and nanocrystalline nature of the samples have been confirmed using X-ray diffractometer and transmission electron microscope. The decrease in oxygen vacancies, local ferromagnetic spin configuration, and breaking of spin cycloid due to smaller size of crystallites are instrumental behind the enhancement of multiferroic properties. Large magnetodielectric coefficient (5.8 % at 1.5 T) for 1Y1Mn combination is observed at room temperature due to enhance coupling between ferromagnetic and ferroelectric ordering achieved by Y and Mn co-doping. We are able to achieve highest saturation magnetization, resistivity, dielectric constant, and lowest dielectric loss in 1Y1Mn co-doped samples compared with both pure BFO and with the other single or co-doped BFO. Our results demonstrate that the co-doping is an effective way to rectify various issues relevant for device applications.

## Introduction

Multiferroic materials, in which ferroelectric and magnetic ordering are present simultaneously, have attracted much attention because of their applications in multiple state memory, electronic field controlled ferromagnetic resonance devices, transducers, and spintronic devices [1–4]. Multiferroics are very rare in nature because the criteria for being simultaneously ferroelectric and ferro/antiferromagnetic are mutually exclusive. Ferroelectricity demands empty d shell in contrast to ferromagnetism where electrons are present in d shell. Among a few known multiferroic materials, perovskite BiFeO$_3$ (BFO), which crystallizes in a rhombohedral distorted structure (space group $R3c$), is unique as it exhibits both ferroelectric and antiferromagnetic (AFM) ordering simultaneously above room temperature [5, 6].

In spite of room temperature multiferroicity, incorporation of BFO in practical devices has been hindered because of large leakage current induced by defects, such as impurities, non-stoichiometry and oxygen vacancies. Low magnetic moment and very weak magneto-electric coupling are other bottlenecks. In order to circumvent these incompatibilities attempts have been made to improve the electrical, optical, and magnetic properties of the BFO materials by ion-doping or by optimizing preparation

A. Mukherjee · S. Basu
Department of Physics, National Institute of Technology, Durgapur, India
e-mail: ayan.mukherjee@phy.nitdgp.ac.in

S. Basu
e-mail: soumen.basu@phy.nitdgp.ac.in

L. A. W. Green · N. T. K. Thanh
Department of Physics and Astronomy, University College London, Gower Street, London, UK
e-mail: law.green.09@alumni.ucl.ac.uk

N. T. K. Thanh
e-mail: thanh-ntk.thanh@ucl.ac.uk

L. A. W. Green · N. T. K. Thanh
UCL Healthcare Biomagnetic and Nanomaterials Laboratories, 21 Albemarle Street, Gower Street, London, UK

M. Pal (✉)
CSIR- Central Glass and Ceramic Research Institute, Kolkata, India
e-mail: palm@cgcri.res.in

parameters [7–14]. However, improvement in magnetic properties without disturbing the ferroelectric properties, as well as a large coupling between ferroelectric and ferromagnetic ordering is essential for their real use in device applications. It is reported that doping of small amount of Mn atoms in the B site of bismuth ferrite ($ABO_3$) can improve the leakage current characteristic and also the magnetic properties [15, 16]. Lin et al. report that doping of Y into the A site of $BiFeO_3$ lattice can also improve the ferroelectric properties [17]. Yet, the weak magnetization of BFO and large leakage current are long-standing problem and various controversial issues are arising from the published literatures [18, 19] which demand more works in this area. Keeping this in mind Y and Mn ion codoped bismuth ferrite ($Bi_{1-x}Y_xFe_{1-y}Mn_yO_3$) nanoparticles synthesized by sol–gel route have been investigated. We are able to achieve enhanced multiferroic properties as well as a large magnetodielectric effect at room temperature as a manifestation of improved magnetoelectric coupling by virtue of codoping. The details are reported here.

## Experimental

### Synthesis

Codoped $BiFeO_3$ ($Bi_{1-x}Y_xFe_{1-y}Mn_yO_3$) ($x = 0.01$, $y = 0.01, 0.05$) are labeled as $BiFeO_3$ (Pure), $Bi_{0.99}Y_{0.01}FeO_3$ (1Y), $BiYFe_{0.99}Mn_{0.01}O_3$ (1Mn), $Bi_{0.99}Y_{0.01}Fe_{0.99}Mn_{0.01}O_3$ (1Y1Mn), $Bi_{0.99}Y_{0.01}Fe_{0.95}Mn_{0.05}O_3$ (1Y5Mn) nanoparticles were prepared by a simple sol–gel method [20] using metal nitrates as precursors. In the first step, precursor solutions were prepared by dissolving 1:1 molar ratio of $Bi(NO_3)_3 \cdot 5H_2O$ (Sigma Aldrich, 99.99 %), $Fe(NO_3)_3 \cdot 9H_2O$ (Sigma Aldrich, 98 % +), $Y(NO_3)_3 \cdot 10H_2O$ (Sigma Aldrich, 99.99 %) and $Mn(NO_3)_2 \cdot 4H_2O$ (Alfa Aesar, 99.9 %) in 20 ml distilled water under continuous stirring. $HNO_3$ was used to maintain the pH of the solution around two. In the second step, malic acid (0.03 mol) was dissolved in distilled water (30 ml) in a separate beaker. Metal nitrate precursor solutions were added to the malic acid under constant sonication. Polyethylene glycol (PEG) in a molar ratio to malic acid of 1:1 was finally added to the solution as a capping agent. The solution was evaporated to dry polyester precursor powder. Finally, the grinded powders were calcined in air at 873 K for 2 h. The schematic of synthesis procedure is shown in Fig. 1.

### Characterization

The formation of $Bi_{1-x}Y_xFe_{1-y}Mn_yO_3$ ($x = 0.01$, $y = 0.01, 0.05$) nanocrystals was confirmed by X-ray diffraction study. X-ray scans of these samples were recorded with an XPert Pro X-ray diffractometer (PAnalytical, Almelo, Netherlands) with nickel-filtered Cu Kα radiation ($\lambda = 1.5414$ Å) in $2\theta$ range from 20° to 70°. The transmission electron microscopy (HRTEM, JEOL 2011) study was performed to confirm the phase formation and particle size of prepared samples. For TEM study the samples were ground in an agate mortar, dispersed in ethanol by sonication and one drop was dried onto a carbon coated copper grid. The ferroelectric phase transitions were studied using a differential thermal analysis (DTA) instrument (NETZSCH STA449 F1-Jupiter). Thermal analysis was performed up to 1173 K with a rate of heating 10 K/min under $N_2$ atmosphere. The magnetic properties of the samples were measured by using superconducting interface device (SQUID) magnetometer MPMS (Quantum Design, USA) fitted with a 7 T magnet.

For electrical measurements, the powder was cold pressed to form a pallet in a steel mold of 1.3 cm diameter and compacted at a pressure of $7 \times 10^4$ Pa. Silver paint electrodes (supplied by Acheson Colloiden B.V. Holland) were applied on two opposite faces. Direct-current (dc) conductivity was measured using Keithley 6514 electrometer. The temperature dependence of conductivity was measured in a furnace fitted with a Eurotherm temperature controller. The ac measurement was performed using an Agilent E4980A LCR meter. Magnetodielectric coefficient was measured by using an electromagnet of 1.5 T.

## Result and discussions

DTA was carried out to check the effect of doping on Curie temperature. The enlarged view of the DTA patterns obtained for different samples in the temperature range from 1050 to 1140 K is shown in Fig. 2a). The endothermic peak around 1098 K is attributed to ferroelectric phase transitions and matches well with published literature [21]. No significant amount of mass loss is observed during this ferro to paraelectric phase transition which is clearly demonstrated in the TGA pattern (Fig. 2b). The ferroelectric phase transition is observed to decrease with the different doping element concentration as summarised in Table 2, which could be a combinatorial effect of a large increase in non-uniform strain and decrease of particle size due to doping. The ferroelectric transition temperature observed for different samples is summarized in Table 1.

Effect of doping on structure has been studied using X-ray diffractometry. The powder diffraction pattern of the prepared samples containing different Y and Mn concentration is delineated in Fig. 3a. All the peaks in the figure are indexed to various planes (hkl) of $BiFeO_3$ and are in good agreement with the literature data (JCPDS Card No. 86-1518), demonstrate the formation of highly pure

Fig. 1 Schematic representation of the material synthesis process
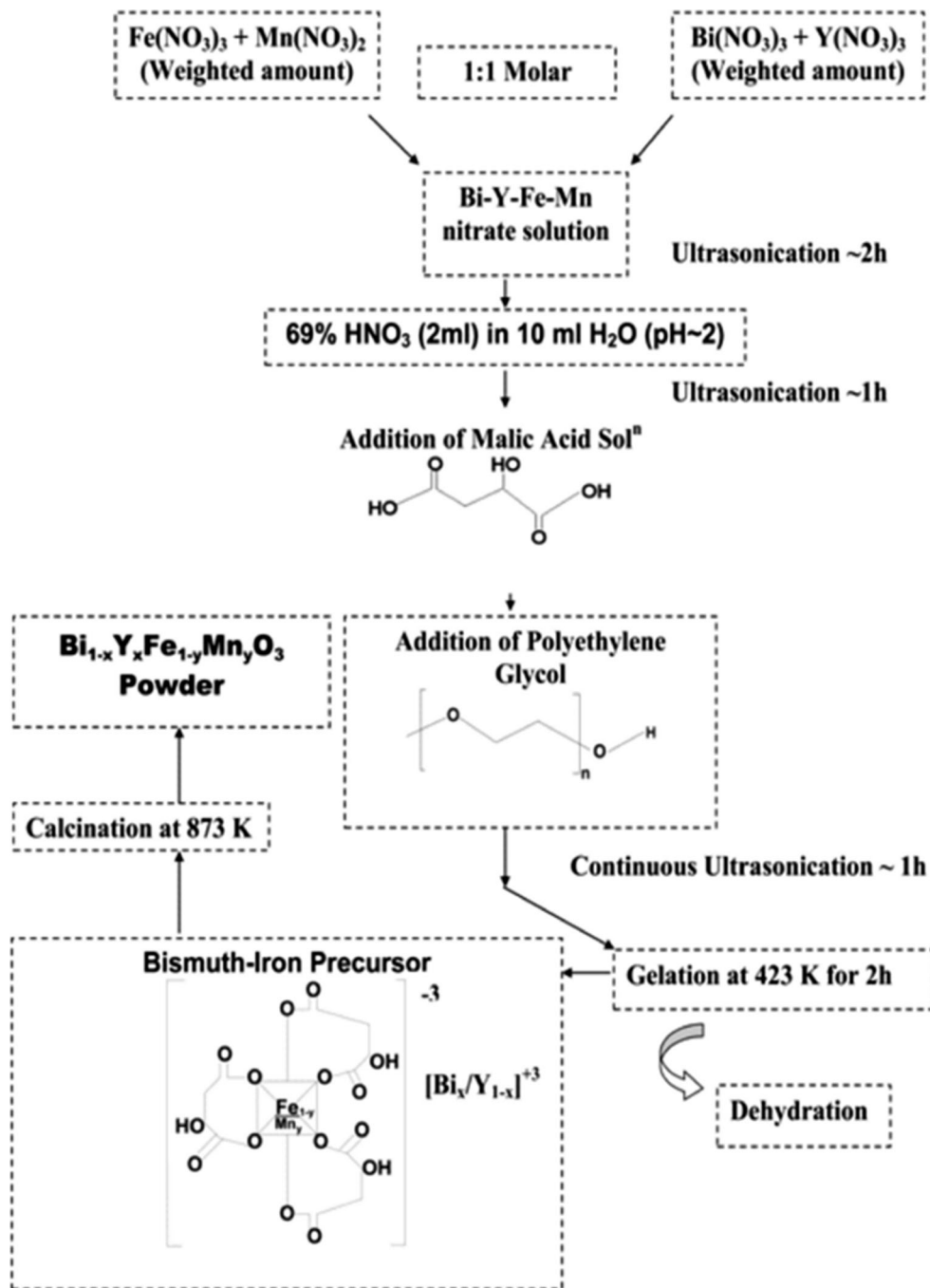
crystalline $Bi_{1-x}Y_xFe_{1-y}Mn_yO_3$ nanoparticles. To observe the doping effect the magnified X-ray diffraction pattern is delineated in Fig. 3b. It is clear that doping has resulted in a peak shift toward low angle side which indicates modification of lattice parameters. BFO nanoparticles have large self-(transformation) strain, the relaxation of the structure around widely separated substituent ions produces local structural distortions that result in diffraction profiles showing strongly asymmetric (and often anisotropic) broadening and modification of lattice parameter. In

this instance, the shifts observed in the peak maxima correspond to a distribution in lattice parameters. In addition, 1 Mn-doped samples show a broad single peak around 32° instead of two peaks, which suggests that the rhombohedral distortion is reduced toward orthorhombic or tetragonal structure [22].

Rietveld refinement has been adopted for complete microstructural characterization of the samples in terms of change in lattice parameter, crystallite size and lattice strain. The refinement has been carried out using the
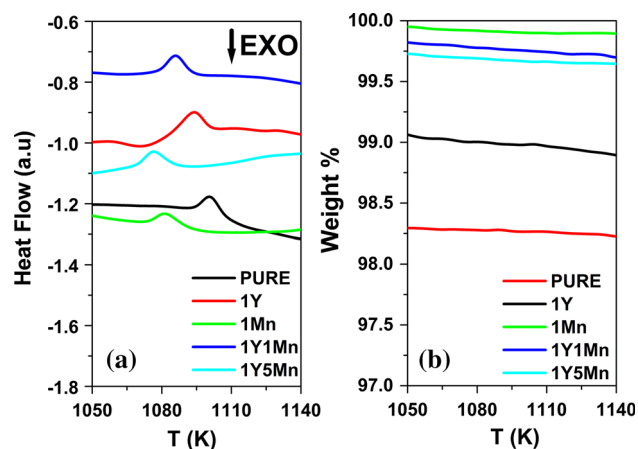
**Fig. 2 a** Enlarged DTA pattern for all samples. **b** Enlarged TGA pattern for all samples

**Table 1** Various electrical and magnetic parameters of all the samples

| Samples | $T_c$ (K) | $M_s$ (emu/gm) | | Activation energy (eV) |
|---|---|---|---|---|
| | | 5 K | 300 K | |
| Pure | 1100 | 2.86 | 2.15 | 0.50 |
| 1Y | 1093 | 3.65 | 2.70 | 0.49 |
| 1Mn | 1081 | 3.91 | 3.00 | 0.73 |
| 1Y1Mn | 1085 | 4.87 | 3.92 | 0.89 |
| 1Y5Mn | 1076 | 3.52 | 2.82 | 0.78 |

trigonal space group $R3c$ with lattice constant, $a = 0.55876$ nm, $b = 0.55876$ nm, and $c = 1.3867$ nm.

The background of each pattern was fitted with a 4° polynomial and the line broadening was fitted by refining the lattice parameters, particle size, and lattice strain. The line broadening and size–strain model was chosen to be Popa LB and Popa rules during the refinement. It has been shown that for a pseudo-Voigt (pV) X-ray line shape and Gaussian microstrain distribution the normalized Fourier transform of pV function used for profile fitting is given below as

$$\frac{z}{z+1}\exp\left[-\left(\frac{(z+1)^2}{16\ln 2}\right)\right] + \frac{1}{z+1}\exp\left[-\frac{z+1}{z^2}\right]$$
$$= \exp\left[-\pi^2 \langle e^2 \rangle D_{\mathrm{eff}}^2 / (2d^2 - 0.5)\right],$$

where $D_{\mathrm{eff}}$ is the effective crystallite size and $\langle e^2 \rangle$ is the mean square microstrain. During microstructure refinement the values of $D_{\mathrm{eff}}$ and $\langle e^2 \rangle$ are adjusted to obtain a minimum residual.

The refinement of the structural parameters is continued till convergence is optimized to a goodness of fit (GoF) between 1.0 and 1.2. We find that the estimated particle size decreases when it is doped. The variation of lattice

constants, particle size, and microstrain for all samples are tabulated in Table 2.

The average particles size of the pure and doped bismuth ferrite samples has also been estimated from TEM study using a standard log-normal distribution. Figure 4a shows a typical micrograph of 1Y1Mn nanoparticles. Particle size distribution as estimated from Fig. 4a is presented in Fig. 4b. The red colored circles in Fig. 4b represent the experimental data point and the black colored line represents the regression fit to a log-normal distribution function. The estimated particle size for different samples was found to be approximately 29 nm. Figure 4c is the high resolution TEM image of 1Y1Mn sample which shows the lattice fringes very clearly. The estimated lattice spacing 2.28 and 1.99 Å corresponding to (012) and (202) planes of $BiFeO_3$ are observed, which reconfirm the growth of well crystalline BFO samples. It is worth mentioning here that a little difference in estimated particle size from two different techniques is observed. Actually, the particle size obtained from XRD analysis due to peak broadening basically gives the crystallite size, which is always less than or equal to the exact particle size. However, both the technique confirms the decrease of particle size due to doping. This may be due to the increase of lattice distortion (confirmed by Rietveld analysis) which resists the growth of nanoparticles. The selected area diffraction SAD presented in Fig. 4d reconfirms well-crystallised nature of 1Y1Mn nanoparticles.

Magnetic studies for all the samples have been carried out and Fig. 5a shows the hysteresis loop at 5 K. Shapes of the curves confirm the ferro/ferrimagnetic nature of the prepared samples. An enlarged view of the hysteresis loops at 5 K for all samples is shown in Fig. 5b. The observed large coercivity values indicate that the samples are not superparamagnetic below the room temperature. It is observed that 1Y1Mn sample shows higher saturation magnetization than other doped samples and may be attributed to the higher lattice strain developed due to beneficial effect of codoping, which also agreed very well with the zero-field-cooled (ZFC) and field-cooled (FC) study (Fig. 6). Figure 5c shows the hysteresis loops of 1Y1Mn sample for different temperatures. Figure 5d is the expanded hysteresis loop at 300 K for the 1Y1Mn sample to delineate coercivity clearly. It is clear from the Fig. 5c that the magnetisation value increases with the decrease in temperature. This is to be expected in the case of ferro/ferrimagnetic particles [23, 24]. A comparison between magnetic parameters is summarised in Table 1.

The temperature dependent magnetization study has been carried out in order to illustrate the effect of doping on magnetic properties in $Bi_{1-x}Y_xFe_{1-y}Mn_yO_3$ nanocrystals. Figure 6 shows the variation of magnetization as a function of temperature under both zero-field-cooled (ZFC) and field-cooled (FC) conditions for the different samples

**Fig. 3 a** XRD pattern of all samples, **b** magnified XRD pattern of all samples in the range (31°–32.5°)
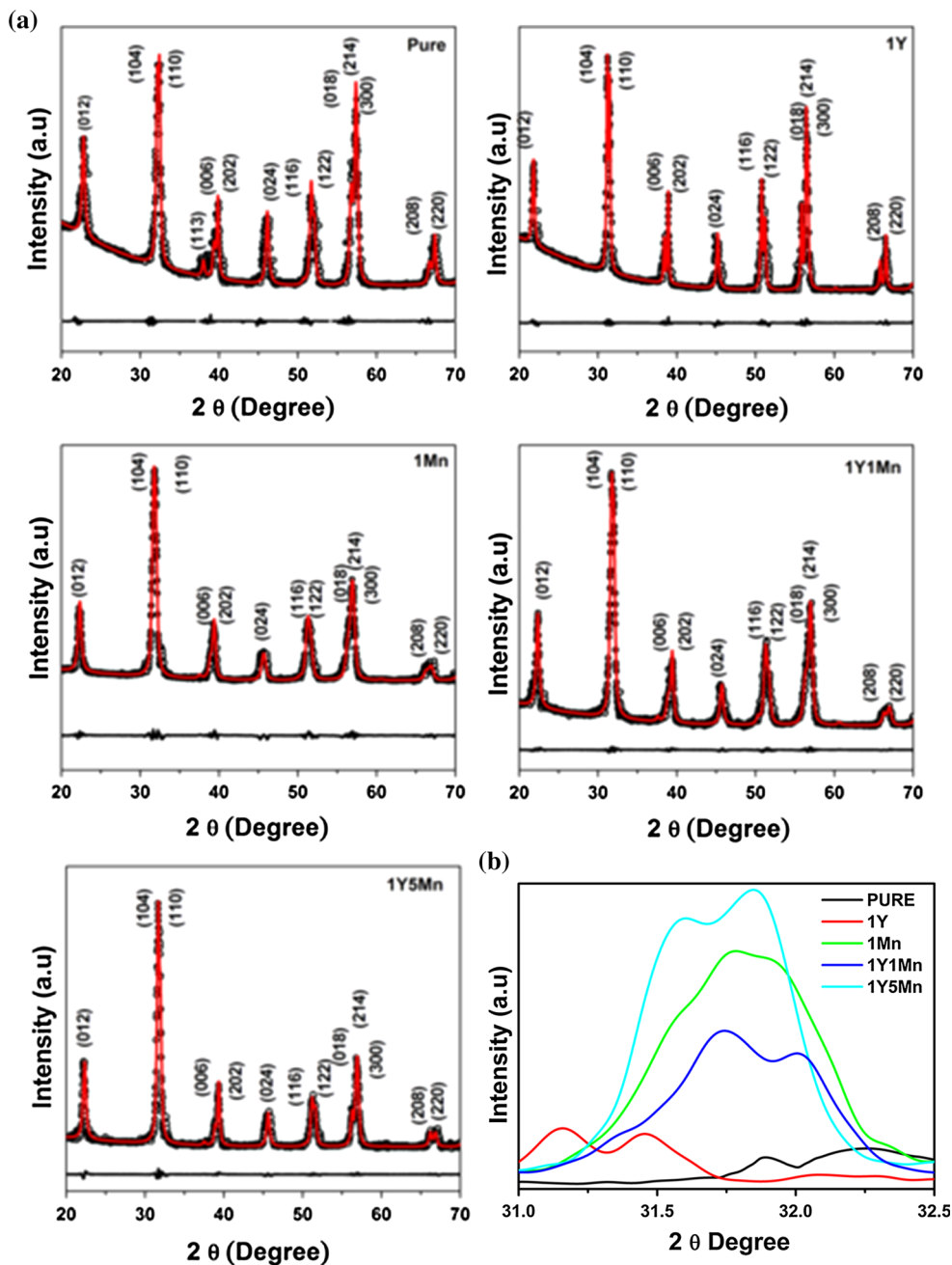


**Table 2** Rietveld refinement parameter for all samples

| Sample | $a$ | $b$ | $c$ | Particle size (nm) | Micro strain $\times 10^{-3}$ |
|--------|------|------|--------|------|------|
| Pure | 5.552 | 5.552 | 13.882 | 33 | 1.67 |
| 1Y | 5.559 | 5.559 | 13.867 | 30 | 2.62 |
| 1Mn | 5.603 | 5.603 | 13.745 | 25 | 6.35 |
| 1Y1Mn | 5.621 | 5.621 | 13.773 | 27 | 8.65 |
| 1Y5Mn | 5.608 | 5.608 | 13.739 | 23 | 6.25 |

in the presence of an applied magnetic field of 100 Oe. A distinct split between the FC and ZFC curves below room temperature (300 K) is observed for all the samples. This split is similar to that found for ferro/ferrimagnetic materials, suggesting that $Bi_{1-x}Y_xFe_{1-y}Mn_yO_3$ becomes ferro/ferrimagnetic when particle size is reduced. It was observed that the values of magnetization increased drastically when doped with Y and Mn. The iron-ion's spin in bulk BFO are aligned antiparallely in (111) direction and

**Fig. 4** **a** TEM image of 1Y1Mn sample where red colored circles represent the experimental data point, the *black colored line* and *points* represent the regression fit to a log-normal distribution function, **b** particle size distribution, **c** HRTEM image of 1Y–1Mn, **d** SAD pattern of 1Y1Mn
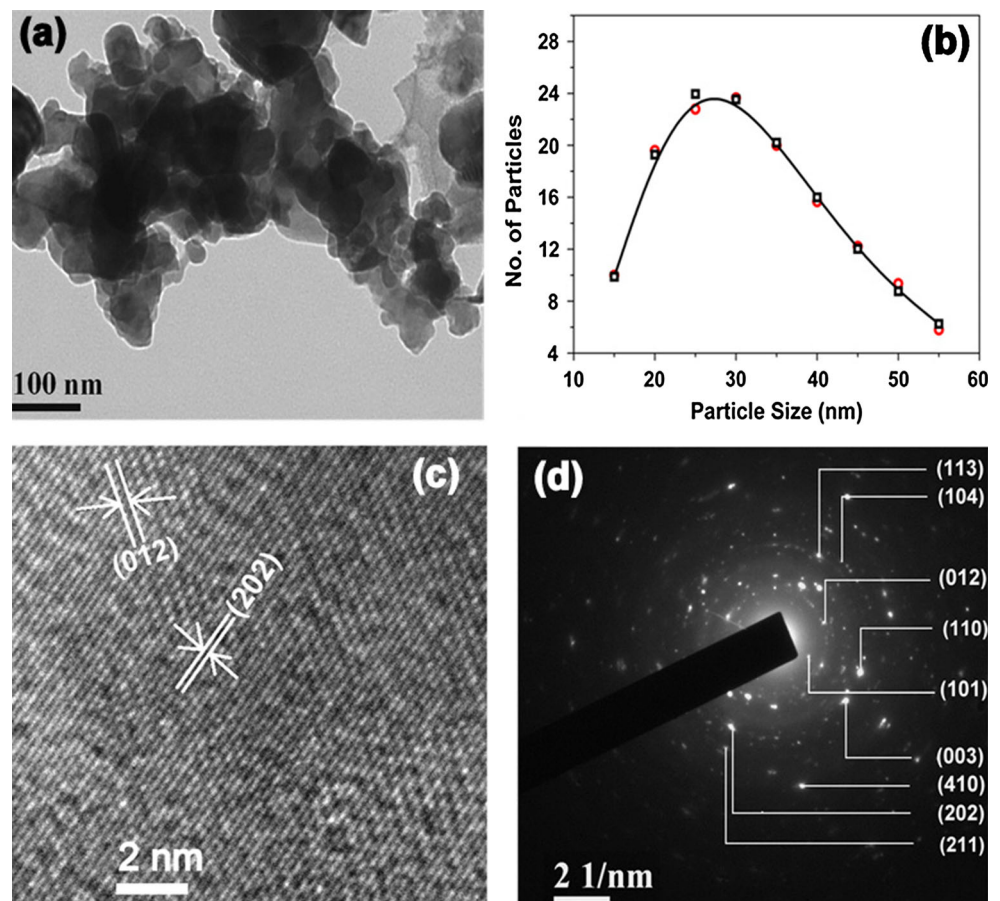


behaves as an antiferromagnetic material. There are two possible explanations for the origin and drastic enhancement of spontaneous magnetization: (i) by substituting iron atoms at the B sites with Mn (other 3*d* transition) atoms, a local ferrimagnetic spin configuration can be expected to form because of the differences in magnetic moment between the B-sites occupants. (ii) Periodicity of the spin cycloid can be broken in small particles when their size is reduced to around or below 62 nm [25].

In order to understand the electrical conduction mechanism, we have performed both dc and ac conductivity studies for all the samples. The ac conductivity of the doped BFO samples has been measured in the temperature range 298 K ≤ T ≤ 523 K and in the frequency range 20 Hz–1 MHz. Figure 7a shows the variation of ac conductivity as a function of frequency for 1Y1Mn sample at different temperatures. All the samples behave in the similar manner. We observe that conductivity strongly depends on frequency as well as temperature and increases almost linearly. Figure 7b delineates the logarithm of dc resistivity variation as a function of inverse temperature. It is clear that all the samples behave like semiconducting material i.e., their resistivity decreases with the increase in temperature. The activation energies estimated from the

slope of the Fig. 7b are found to vary in the range of 0.50–0.89 eV (Table 1). It is observed that the resistivity of bismuth ferrite increases more than four orders of magnitude when doped.

Specially, 1Y1Mn exhibits the highest resistivity of the codoped. This can be explained as incorporation of yttrium and manganese ions in bismuth ferrite lattice may create a large lattice distortion (shifting of X-ray diffraction peaks toward lower angle may confirm this, as shown in Fig. 3b) which will increase the effective potential barrier height for charge carrier contributed in conduction process.

Figure 8a shows the variation of dielectric constant with temperature for different samples at a fixed frequency of 100 kHz. It is observed that with doping the dielectric constant of the samples increases and the 1Y1Mn codoped samples exhibits the highest dielectric constant. This could be the result of a reduced number of oxygen vacancies due to codoping. Higher dielectric constant means lower leakage current which is very much essential for device applications. The variation of tan δ (dielectric loss) up to 523 K for all the samples has been shown in Fig. 8b. Results indicate that tan δ value is very low in the whole temperature range. In addition, results show that by virtue of codoping it is possible to decrease tan δ value further.

Fig. 5 a Hysteresis loop at 5 K for all samples, b Enlarged view of hysteresis loop at 5 K for all samples. c Hysteresis loop for 1Y1Mn at different temperatures. d Enlarged view of hysteresis loop at 300 K for 1Y1Mn
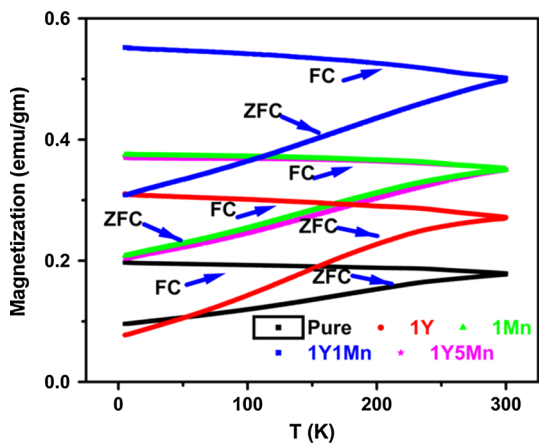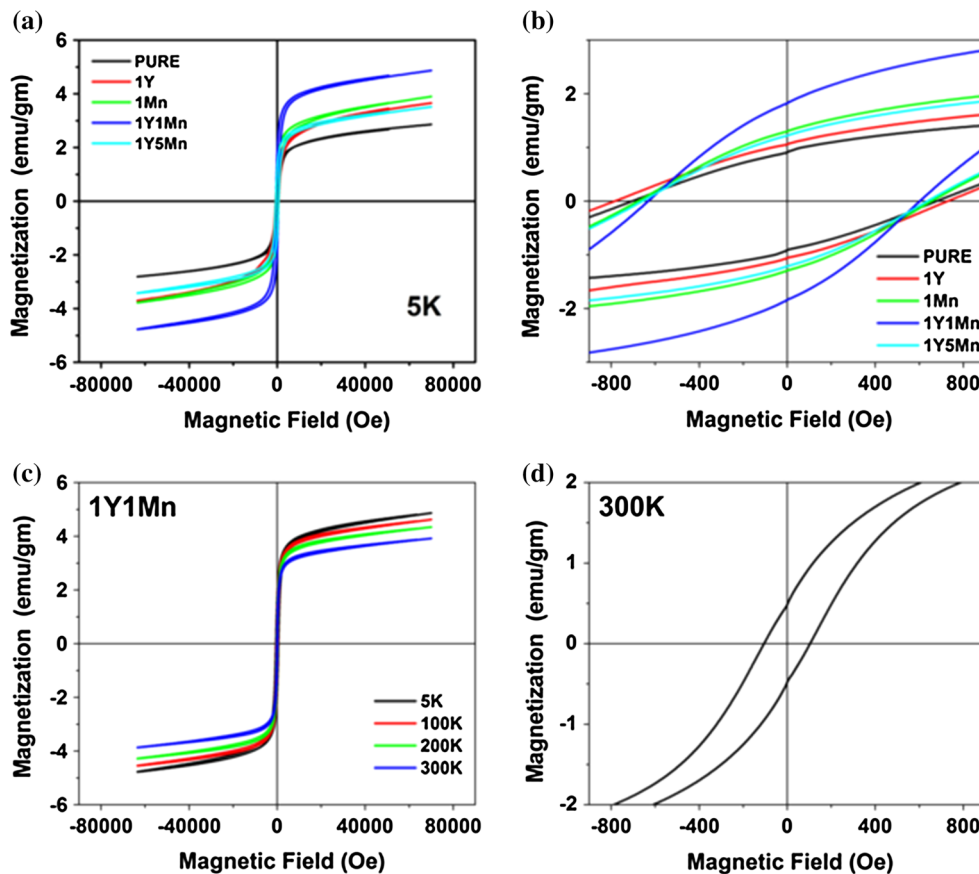




Fig. 6 FC–ZFC curve for all samples

Thus, by proposed codoping it is possible to tackle the leakage current issue of BFO.

Figure 8c shows the variation of dielectric constant with frequency for the 1Y1Mn codoped samples at few selective temperatures. All the samples show similar behavior i.e., dielectric constant is larger at lower frequency region and increases with increase in temperature. Generally, the interfacial polarization occurs due to structural inhomogeneities and the presence of free charges, the hopping

electron is trapped by the inhomogeneities at low frequencies. With the increase in temperature the resistance of the samples decreases while dielectric constant increases at constant frequency. At low resistance, hopping of electrons increases and hence results in larger polarizability or larger dielectric constant. At a fixed temperature, there is a sharp increase in dielectric constant in the low frequency regions because of the existence of large degree of dispersion due to charge transfer within the interfacial diffusion layer present between the electrodes. The magnitude of this dielectric dispersion is temperature dependant. In the low temperature region, the freezing of the electric dipoles are much easier through the relaxation process due to a decay in polarization with respect to the applied electric field. As a result, a sharp decrease in dielectric constant at lower frequency region is observed. In high temperature region quick rate of polarization takes place and hence relaxation occurs at higher frequency. Hence, the inhomogeneous nature of the samples having different permittivity and conductivity regions governs the frequency behavior of dielectric constant where the charge carriers are blocked by the poorly conducting regions. Figure 8d shows the variation of dielectric loss with frequency at different temperature for 1Y1Mn.
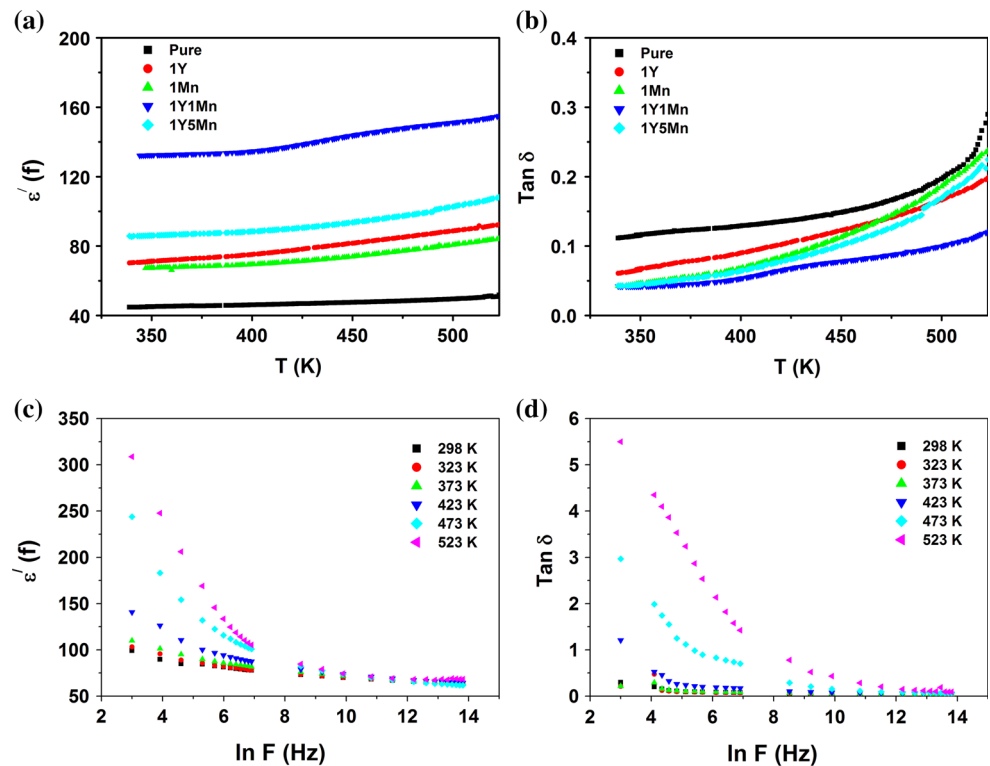
Figure 9 shows the field emission scanning electron micrograph (FESEM) of 1Y1Mn pallet. The volume fraction of the bismuth ferrite phase is found to be 0.76 and the rest is void space. The bright region in the micrograph corresponds the bismuth ferrite phase and the dark region corresponds the void space. It is clearly observed that the bismuth ferrite particles have a volume fraction above the percolation threshold.

The room temperature magnetodielectric coupling of the samples are illustrated by measuring the dielectric constant in the presence of magnetic field in the range $0 \leq H \leq 1.5$ T at a fixed frequency of 100 kHz and delineates in
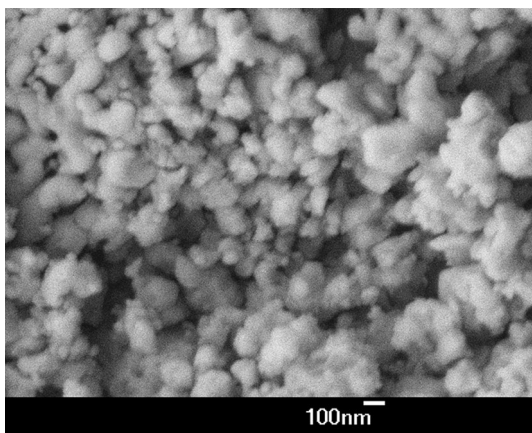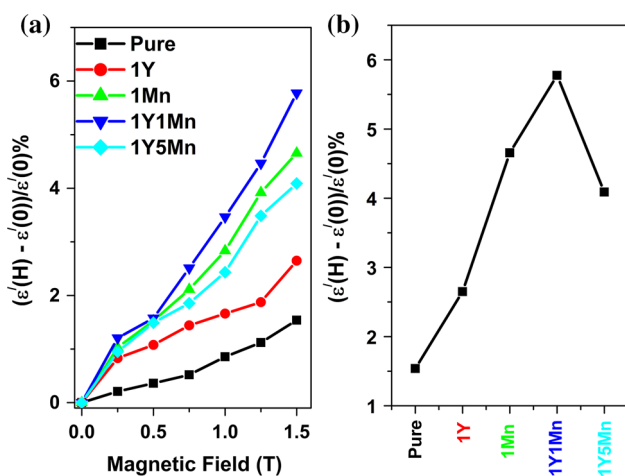
**Fig. 9** FESEM image of 1Y1Mn sample



**Fig. 10 a** Variation of dielectric permittivity with magnetic field. **b** Variation of magnetodielectric coefficient with different samples

ferroelectrics materials) leading to change in dielectric permittivity/polarization.

Our study demonstrates that by a suitable combination of codoping, it is possible to enhance the multiferroic properties of nanocrystalline BFO to a great extent which will be very much beneficial for device applications.

## Conclusions

We have achieved enhanced multiferroic properties in chemically prepared nanocrystalline BFO by codoping. XRD and HRTEM results ruled out the existence of any impurity in the prepared samples. The observed enhancement of magnetization is considered to be related to the combined effect of local ferromagnetic spin configuration and broken spin cycloid due to smaller size. In addition, drastic increase of resistivity in codoped samples attributed to the decrease of charge (oxygen and bismuth) vacancies and increase of effective potential barrier height for charge carrier contributed in conduction process because of codoping. Large magnetodielectric coefficient (5.8 % at 1.5 T) for 1Y1Mn combination was obtained at room temperature, which established the improvement of magnetoelectric coupling by codoping. It implies that the both the register component and breakdown properties are enhanced significantly. It is concluded that yttrium–manganese codoping in BFO nanoparticle is an effective technique to enhance multiferroic properties. However, further research is needed to exactly pin down the reason.

Fig. 10a. The magnetodielectric coefficient (MD%) is represented by the relation

$$\text{MD\%} = \frac{\varepsilon'(H) - \varepsilon'(0)}{\varepsilon'(H)} \times 100,$$

where $\varepsilon'(H)$ and $\varepsilon'(0)$ are the dielectric constants at applied magnetic field and zero field, respectively. The MD coefficient is found to increase for all doped samples and is highest for 1Y1Mn sample (5.8 % at 1.5 T), almost four times larger than pure $BiFeO_3$, which is also much larger than previous reports (2.2, 1 and 2 % for Eu-, Ba-, and Ho-doped BFO, respectively) [26–28]. The variation of magnetodielectric coefficient for different samples is shown in Fig. 10b. The reason for the enhancement of MD coefficient in the codoped system is due to the enhancement of magnetoelectric coupling through lattice distortion of BFO. In magnetoelectric materials, when a magnetic field is applied, the materials will be strained. This strain develops stress in the material (for piezoelectric and

## References

1. Ryu J, Priya S, Uchino K, Kim HE (2002) Magnetoelectric effect in composites of magnetostrictive and piezoelectric materials. J Electroceram 8(2):107–120
2. Wang J, Neaton JB, Zheng H, Nagarajan V, Ogale SB, Liu B, Viehland D, Vaithyanathan V, Schlom DG, Waghmare UV, Spaldin NA, Rabe KM, Wuttig M, Ramesh R (2003) Epitaxial $BiFeO_3$ multiferroic thin film heterostructures. Science 299:1719–1722
3. Fiebig M, Lottermoser T, Fröhlich D, Goltsev AV, Pisarev RV (2002) Observation of coupled magnetic and electric domains. Nature 419:818–820
4. Kanai T, Ohkoshi SI, Nakajima A, Watanabe T, Hashimoto K (2001) A ferroelectric ferromagnet composed of $(PLZT)_x(BiFeO_3)_{1-x}$ solid solution. Adv Mater 13:487–490

5. Cheng ZX, Wang XL, Kannan CV, Ozawa K, Kimura H, Nishida T, Zhang SJ, Shrout TR (2006) Enhanced electrical polarization and ferromagnetic moment in a multiferroic $BiFeO_3/Bi_{3.25}Sm_{0.75}Ti_{2.98}V_{0.02}O_{12}$ double-layered thin film. Appl Phys Lett 88:132909

6. Dho J, Qi X, Kim H, MacManus-Driscoll JL, Blamire MG (2006) Large electric polarization and exchange bias in multiferroic $BiFeO_3$. Adv Mater 18:1445–1448

7. Mukherjee A, Basu S, Chakraborty G, Pal M (2012) Effect of Y-doping on the electrical transport properties of nanocrystalline $BiFeO_3$. J Appl Phys 112:014321–014328

8. Mukherjee A, Hossain SKM, Basu S, Pal M (2012) Effect of Y-doping on optical properties of multiferroics $BiFeO_3$ nanoparticles. Appl Nanosci 2:305–310

9. Xiaomeng L, Jimin X, Yuanzhi S, Jiamin L (2007) Surfactant-assisted hydrothermal preparation of submicrometer-sized two-dimensional $BiFeO_3$ plates and their photocatalytic activity. J Mater Sci 46:6824–6827. doi:10.1007/s10853-006-1401-0

10. Basu S, Hossain SKM, Chakravorty D, Pal M (2011) Enhanced magnetic properties in hydrothermally synthesized Mn-doped $BiFeO_3$ nanoparticles. Curr Appl Phys 11:976–980

11. Hossain SKM, Mukherjee A, Chakraborty S, Yusuf SM, Basu S, Pal M (2013) Enhanced multiferroic properties of nanocrystalline La-doped $BiFeO_3$. Mater Focus 2:1–7

12. Casper MD, Losego MD, Maria J-P (2013) Optimizing phase and microstructure of chemical solution-deposited bismuth ferrite ($BiFeO_3$) thin films to reduce DC leakage. J Mater Sci 48:1578–1584. doi:10.1007/s10853-012-6914-0

13. Khomchenko VA, Troyanchuk IO, Karpinsky DV, Paixão JA (2012) Structural and magnetic phase transitions in $Bi_{1-x}Pr_xFeO_3$ perovskites. J Mater Sci 47:1578–1581. doi:10.1007/s10853-011-6040-4

14. Chybczyńska K, Ławniczak P, Hilczer B, Łęska B, Pankiewicz R, Pietraszko A, Kępiński L, Kałuski T, Cieluch P, Matelski F, Andrzejewski B (2014) Synthesis and properties of bismuth ferrite multiferroic flowers. J Mater Sci 49:2596–2604. doi:10.1007/s10853-013-7957-6

15. Gupta S, Tomar M, James AR, Gupta V (2014) Ce-doped bismuth ferrite thin films with improved electrical and functional properties. J Mater Sci 49:5355–5364. doi:10.1007/s10853-014-8243-y

16. Singh SK, Ishiwara H, Maruyama K (2006) Room temperature ferroelectric properties of Mn-substituted $BiFeO_3$ thin films deposited on Pt electrodes using chemical solution deposition. Appl Phys Lett 88:262908

17. Lin FB, Hau X, Xian XZ (2010) Structure and multiferroic properties of Y-doped $BiFeO_3$ ceramics. Chin Sci Bull 55:452–456

18. Wu J, Wang J, Xiao D, Zhu J (2011) Ferroelectric behavior in bismuth ferrite thin films of different thickness. ACS Appl Mater Interfaces 3:3261–3263

19. Silva J, Reyes A, Castañeda R, Esparza H, Camacho H, Matutes J, Fuentes L (2012) Structure and electromagnetic properties of $Bi_{1-x}Y_xFe_{0.95}Mn_{0.05}O_3$ (x = 0.05, 0.075 and 0.10). Ferroelectrics 426:103–111

20. Pechini MP (1967) US Patent No. 3.330.697. July 1 1967

21. Wang YP, Yuan GL, Chen XY, Liu JM, Liu ZG (2006) Electrical and magnetic properties of single-phased and highly resistive ferroelectromagnet $BiFeO_3$ ceramic. J Phys D Appl Phys 39:2019

22. Yang KG, Zhang YL, Yang SH, Wang B (2010) Structural, electrical, and magnetic properties of multiferroic $Bi_{1-x}La_xFe_{1-y}Co_yO_3$ thin films. J Appl Phys 107:124109–124114

23. Park TJ, Papaefthymiou GC, Viescas AJ, Moodenbough AR, Wong SS (2007) Size-dependent magnetic properties of single-crystalline multiferroic $BiFeO_3$ nanoparticles. Nano Lett 7:766–772

24. Frei EH, Shtrikman S, Treves D (1957) Critical size and nucleation field of ideal ferromagnetic particles. Phys Rev 106(3):446–455

25. Pal M, Chakravorty D (2003) Nanocrystalline magnetic alloys and ceramics. Sadhana 28(1–2):283–297

26. Zhang X, Sui Y, Wang X, Wang Y, Wang Z (2010) Effect of Eu substitution on the crystal structure and multiferroic properties of $BiFeO_3$. J Alloys Compd 507:157–161

27. Wang DH, Goh WC, Ning M, Ong CK (2006) Effect of Ba doping on magnetic, ferroelectric, and magnetoelectric properties in mutiferroic $BiFeO_3$ at room temperature. Appl Phys Lett 88:212907–212909

28. Uniyal P, Yadav KL (2012) Enhanced magnetoelectric properties in $Bi_{0.95}Ho_{0.05}FeO_3$ polycrystalline ceramics. J Alloys Compd 511:149–153